Dyes and Pigments 104 (2014) 197–203

Contents lists available at ScienceDirect

Dyes and Pigments

journal homepage: www.elsevier.com/locate/dyepig

Facile synthesis of metal-free organic dyes featuring a thienylethynyl spacer for dye sensitized solar cells☆

Manal Al-Eid [a,1], SungHwan Lim [b,1], Kwang-Won Park [b,1], Brian Fitzpatrick [a], Chi-Hwan Han [c], Kyungwon Kwak [b,**], Jongin Hong [b,***], Graeme Cooke [a,*]

[a] Glasgow Centre for Physical Organic Chemistry, WestCHEM School of Chemistry, University of Glasgow, Glasgow G12 8QQ, UK
[b] Department of Chemistry, Chung-Ang University, Seoul 156-756, Republic of Korea
[c] Photovoltaic Research Center, Korea Institute of Energy Research, Daejeon 305-343, Republic of Korea

ARTICLE INFO

Article history:
Received 7 November 2013
Received in revised form
19 December 2013
Accepted 3 January 2014
Available online 12 January 2014

Keywords:
Dye-sensitized solar cells
Organic dye
Metal-free
Thiophene
Solvatochromic
Alkyne

ABSTRACT

In this article, we report the facile synthesis of metal-free dyes **6** and **7**, their solution-based optical and redox properties and their use as sensitizers in dye-sensitized solar cells (DSSCs). Our studies indicate that the addition of the second thiophene unit in dye **7**, decreases the oxidation and reduction potential and consequently the band gap of the molecule compared to **6**. Furthermore, increasing the length of the conjugated spacer also affects on the properties of the DSSCs, with dye **7** providing a higher power conversion efficiency compared to **6** (η = 4.49 versus 3.23%).

1. Introduction

Dye-sensitized solar cells (DSSCs) are attracting significant academic and commercial interest as possible lower-cost alternatives to conventional solid-state photovoltaic devices [1,2]. The nature of the photosensitizer plays an important role in DSSCs, as it has a profound influence on both the power conversion efficiency as well as the stability of the cells. Organic dyes have attracted much interest in recent years as they offer several advantages over their ruthenium-based brethren including bespoke structural modification through rich synthetic protocols, lower cost large-scale production, reduced environmental and toxicity issues and high molar extinction coefficients [3–7]. One of the main goals in this area has been focused upon improving the power-conversion-efficiency of these systems through structural modification [8]. In general, these systems feature donor (D) and acceptor (A) systems separated by a π-conjugated bridge (D–π–A). For example, triphenylamine derivatives have been commonly utilized as the electron donor (D), whilst a cyanoacrylic acid moiety acts as the electron acceptor (A) and anchoring unit in the D–π–A structure [9]. Various π-conjugated bridges, such as benzene, thiophene and benzothiadiazole, have been introduced to broaden their absorption towards the near-infrared region. Interestingly, studies have shown that in addition to optimizing the optical properties of the dye, increasing the number of thiophene π-bridging units tends to result in an increase in power conversion efficiency [10]. Another important goal is to develop systems that may be accessed through short and simple synthetic routes for more widespread implementation in lower cost applications [11].

In this study, we report the facile synthesis of two organic dyes (**6** and **7**, Scheme 1), which can be conveniently prepared in two steps from commercially available thiophene derivatives **1** and **2** and alkyne **3**. The dyes have been designed to investigate the effect of increasing conjugation through the addition of thiopehene units has on the properties of the dyes. Importantly, the acetylene linker

* Corresponding author. Tel.: +44 141 3305500.
** Corresponding author. Tel.: +82 28205764.
*** Corresponding author. Tel.: +82 28205869.
E-mail addresses: kkwak@cau.ac.kr (K. Kwak), hongj@cau.ac.kr (J. Hong), Graeme.Cooke@glasgow.ac.uk (G. Cooke).
[1] Equal contribution to this work.

0143-7208/$ – see front matter © 2014 The Authors. Published by Elsevier Ltd. All rights reserved.
http://dx.doi.org/10.1016/j.dyepig.2014.01.004

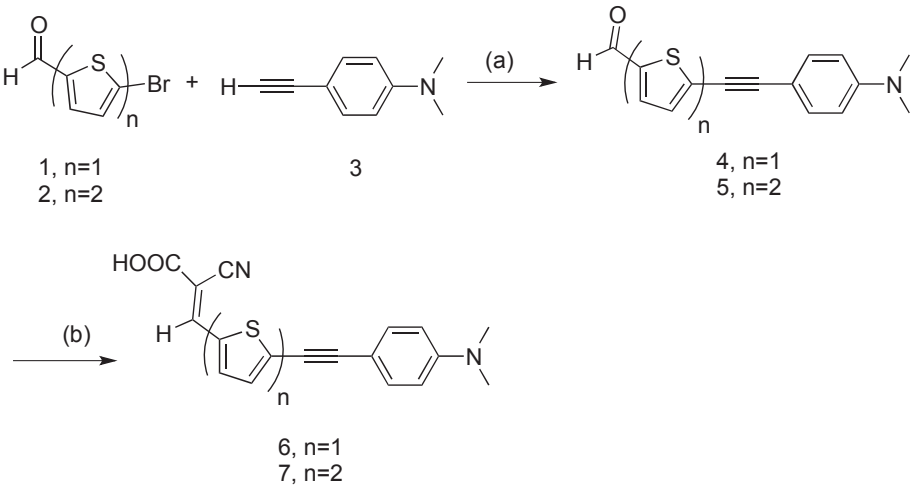

Scheme 1. Reagents and conditions: (a) Pd/C 10%, CuI, Ph_3P, K_2CO_3, DME: H_2O; (b) cyanoacetic acid, piperidine, CH_3CN.

group has been included to provide a planar linker moiety [12–14] and as a handle for further synthetic manipulation [15]. We have investigated the influence the number of thiophene units has on the optical, redox and DSSC properties of dyes **6** and **7**. This study has revealed that the addition of the second thiophene unit in compound **7** plays an important role in modulating the optical and redox properties of this system compared to **6**. Furthermore, increasing the conjugation between the D and A units in this way also results in improved efficiency of the DSSCs (**6** $\eta = 3.23\%$; **7** $\eta = 4.49\%$).

2. Experimental

2.1. Materials

All reactions were undertaken under a nitrogen atmosphere. Solvents were purified using a PureSolv solvent purifier system. Compounds **1**, **2** and **3** were purchased from either Aldrich or TCI, and were used without further purification.

2.2. Characterization

NMR spectroscopy was undertaken on a Bruker AVIII (400 MHz) spectrometer. Chemical shifts are reported in ppm and are relative to tetramethylsilane. UV–vis spectra were recorded on a Perkin–Elmer Lamda 25 instrument. Band gaps (E_g) were estimated using the absorption edge of the longest wavelength absorption (λ) using $E_g = 1240/\lambda$. Cyclic voltammetry measurements were undertaken using a CH Instruments 440a electrochemical analyzer using a platinum disc working electrode, a platinum wire counter electrode and a silver wire pseudo-reference electrode. Ferrocene was used as an internal standard and all redox couples are reported versus the ferrocene/ferrocenium (Fc/Fc^+) redox couple adjusted to 0.0 V. The solutions were prepared using dry dimethylformamide (DMF) containing electrochemical grade tetrabutylammonium hexafluorophosphate (0.1 M) as the supporting electrolyte. The solutions were purged with nitrogen gas for 3–4 min prior to recording the electrochemical data. The HOMO/LUMO energies were estimated from the oxidation and reduction waves, respectively, using a HOMO energy for ferrocene of −4.8 eV [16].

2.3. Computation

Density functional theory (DFT) and time-dependent density functional theory (TDDFT) calculations were performed using a Gaussian '09 software package [17]. The geometry of dyes **6** and **7** was optimized using the B3LYP method with the 6–31 + G(d) basis set. The optimized structures have been classified as local minima on their respective potential energy surfaces according to their vibrational frequencies. None of the vibrational frequencies in the optimized geometries generated negative frequencies in their ground state. To introduce the effect of solvent, the electronic states of both organic dyes in acetonitrile were also calculated by means of the Tomasi's Polarized Continuum Model (PCM).

2.4. Synthesis

2.4.1. Compound *4*

5-Bromo-2-thiophenecarboxaldehyde **1** (0.50 g, 2.30 mmol), 10% Pd/C (0.07 g, 0.07 mmol), CuI (0.13 g, 0.68 mmol), Ph_3P (0.47 g, 1.80 mmol) and K_2CO_3 (0.50 g, 3.6 mmol) were dissolved at room temperature in a 1:1 mixture of water (15 mL) and DME (15 mL). The mixture was degassed with N_2 for 5 min and stirred for 30 min under N_2. Then 4-ethynyl-N,N-dimethylaniline **3** (0.50 g, 3.40 mmol) was added to the mixture. The reaction mixture was heated under reflux overnight. The mixture was then cooled and DCM (80 mL) was added and the organic layers were separated, dried over $MgSO_4$ and filtered. The solvent was evaporated under reduced pressure and the residue was purified by column chromatography (SiO_2; toluene/DCM, 9:1) to give **4** as an orange solid (0.37 g, 63%); mp. 147–149 °C; ^1H NMR (400 MHz, $CDCl_3$) δ 9.84 (s, 1H), 7.64 (d, J = 3.9 Hz, 1H), 7.41 (d, J = 8.9 Hz, 2H), 7.22 (d, J = 3.9 Hz, 1H), 6.65 (d, J = 8.9 Hz, 2H), 3.02 (s, 6H) ppm; ^{13}C NMR (100 MHz, $CDCl_3$) δ 182.2 (C=O), 150.7 (C–N), 142.7 (C–H), 136.3 (C–H), 134.4 (C–C), 132.9 (2 × C–H), 131.2 (C–H), 111.6 (2 × C–H), 108.1 (C–C), 100.3 (C≡C), 80.6 (C≡C), 40.0 (2 × C–N) ppm; IR (film) υ 2807, 2182, 1656, 1229 cm^{-1}; HRMS m/z (EI+) calculated for $C_{15}H_{13}NOS$ 255.0718 found 255.0708.

2.4.2. Compound *5*

5-Bromo-2,2′-bithiophene-5′-carboxaldehyde **2** (0.50 g, 1.83 mmol), 10% Pd/C (0.06 g, 0.06 mmol), CuI (0.10 g, 0.55 mmol), Ph_3P (0.40 g, 1.50 mmol) and K_2CO_3 (0.40 g, 2.90 mmol) were dissolved at room temperature in a 1:1 mixture of water (15 mL) and DME (15 mL). The mixture was degassed with N_2 for 5 min and stirred for 30 min under N_2. Then 4-ethynyl-N,N-dimethylaniline **3** (0.40 g, 2.75 mmol) was added to the mixture. The reaction mixture was heated under reflux overnight. The mixture was then cooled and DCM (80 mL) was added and the organic layers were separated,

dried over $MgSO_4$ and filtered. Then the solvent was evaporated under reduced pressure and the residue was then purified by column chromatography (SiO_2; DCM/petroleum ether, 9:1) to give **5** as an orange solid (0.37 g, 40%); mp. 200–203 °C; ^{1}H NMR (400 MHz, $CDCl_3$) δ 9.86 (s, 1H), 7.66 (d, J = 4.0 Hz, 1H), 7.39 (d, J = 8.9 Hz, 2H), 7.23 (d, J = 3.4 Hz, 1H), 7.22 (d, J = 3.4 Hz, 1H), 7.13 (d, J = 4.0 Hz, 1H), 6.66 (d, J = 8.9 Hz, 2H), 3.01 (s, 6H) ppm; ^{13}C NMR (100 MHz, $CDCl_3$) δ 182.4 (C–H), 150.4 (C–C), 146.6 (C–C), 141.6 (C–C), 137.3 (C–H), 135.8 (C–C), 132.7 (2 × C–H), 131.8 (C–H), 126.3(C–C), 126.0 (C–H), 124.2 (C–H), 111.7 (2 × C–H), 108.8 (C–C), 97.3 (C≡C), 80.2 (C≡C), 40.1 (2 × CH_3–N) ppm; IR (film) υ 2787, 2185, 1654, 1228 cm^{-1}; HRMS m/z (EI^+) calculated for $C_{19}H_{15}NOS_2$ 337.0595 found 337.0591.

2.4.3. Dye **6**

To a mixture of compound **4** (0.40 g, 1.80 mmol) and cyanoacetic acid (0.30 g, 3.60 mmol) in CH_3CN (20 mL) was added piperidine (0.2 mL). The reaction mixture was heated under reflux overnight under nitrogen. After cooling to room temperature, the mixture was then poured into (1 *N*) HCl and chloroform (200 mL) was added. The organic layer was separated and washed with brine, water and dried over $MgSO_4$ and filtered. Then solvent was evaporated and the crude product was purified by column chromatography (SiO_2: chloroform/acetic acid, 9:1) to afford **6** as a red solid (0.18 g, 31%); mp. 210–220 °C; ^{1}H NMR (500 MHz, DMSO) δ 8.48 (s, 1H), 7.96 (d, J = 4.0, 1H), 7.45 (d, J = 4.0, 1H), 7.42 (d, J = 9.1, 2H), 6.73 (d, J = 9.1, 2H), 2.98 (s, 6H) ppm; ^{13}C NMR (125 MHz, DMSO) δ 163.2 (C–OOH), 150.9 (C–N phen), 145.6 (C–H), 139.7 (C–H), 135.5 (C–C), 132.8 (2 × C–H), 132.0 (C–H), 131.8 (C–C), 116.5 (C≡N), 111.9 (2 × C–H), 106.7 (C–C), 101.1 (C=CN,COOH), 81.3 (C≡C), 80.7 (C≡C), 39.9 (2 × C–N) ppm; IR (film) υ 3200, 2177, 1680, 1600 cm^{-1}; HRMS (FAB (M + Na)$^+$) calculated for C_{18} H_{14} N_2 O_2 S Na 345.0674 found 345.0676.

2.4.4. Dye **7**

To a mixture of compound **5** (0.40 g, 1.20 mmol) and cyanoacetic acid (0.20 g, 2.40 mmol) in CH_3CN (20 mL) was added piperidine (0.2 mL). The reaction mixture was heated under reflux overnight under nitrogen. After cooling to room temperature, the mixture was then poured into (1 *N*) HCl and the chloroform (200 mL) was added. The organic layer was separated and washed with brine, water, dried over $MgSO_4$ and filtered. Then solvent was evaporated and the crude product was purified by column chromatography (SiO_2: chloroform/acetic acid, 9:1) to afford **7** as a red solid (0.10 g, 28%); mp. 235–245 °C; ^{1}H NMR (400 MHz, DMSO) δ 8.40 (s, 1H), 7.92 (d, J = 4.0, 1H), 7.58 (d, J = 4.0, 1H), 7.54 (d, J = 4.0, 1H), 7.37 (d, J = 8.9, 2H), 7.33 (d, J = 4.0, 1H), 6.73 (d, J = 8.9, 2H), 2.97 (s, 6H) ppm; IR (film) υ 3308, 2177, 1633, 1604 cm^{-1}; HRMS (FAB (M-H)$^-$) calculated for $C_{22}H_{16}N_2O_2S_2$ 403.0574 found 403.0561.

2.4.5. Fabrication of DSSCs and photovoltaic measurements

In order to form artificial pores in the TiO_2 photoanode films, acetylene-black TiO_2 pastes were prepared using a paste-blending method. First, a TiO_2 colloidal solution, which was synthesized by the hydrothermal growth method, was used for the starting material. Both ethylene carbonate and terpineol were added in the solution and all were mixed by using a paste blender. Then, acetylene-black powder (Chevron Philips Chemical Company) was blended. The mixed paste was concentrated at 80 °C for 2 h using a rotary evaporator to achieve appropriate viscosity for screen printing. More details about its preparation can be found in Ref. [18]. The acetylene-black TiO_2 paste was screen-printed on transparent fluorine-doped SnO_2 (FTO) conducting glass (TEC 8, sheet resistance = 8 Ω/sq) which were purchased from Pilkington. The resultant layer was dried for 10 min at 300 °C in air on a pre-heated hot plate. The screen printing and drying process was repeated twice until a thickness of about 20 μm was obtained. The TiO_2 thick films were gradually heated to 300 °C over 30 min period under an airflow, heated at 300 °C for 1 h, heated to 575 °C over 30 min period, and then finally sintered at 575 °C for 1 h in a muffle furnace and then cooled to room temperature. Active areas of the electrodes were 0.25 cm^2. The prepared TiO_2 electrodes were immersed in a 0.04 M $TiCl_4$ solution at 70 °C for 1 h [19]. They were rinsed with water and ethanol and then sintered at 500 °C for 30 min. The TiO_2 electrodes were exposed to an O_2 plasma and then immersed into a 0.5 mM photosensitizer solution (ethanol) (**N719**, compound **6**, compound **7**) for 24 h. Pt-counter electrodes were prepared on the FTO glass by magnetron sputtering after two holes were drilled in the glass. Both the photosensitizer-adsorbed TiO_2 electrode and the Pt-counter electrode were sealed with 60 μm-thick Surlyn (Solaronix). An ionic liquid electrolyte (0.60 M butylmethyl imidazolium iodide (BMIM-I), 0.03 M I_2, 0.50 M 4-tert-butylpyridine (TBP) and 0.10 M guanidinium thiocyanate (GTC) in acetonitrile/valeronitrile 85/15 (v/v), No. ES-0004, io·li·tec, Germany) was filled through the holes in the backside of the counter electrode. The photovoltaic characteristics of the devices under AM 1.5 global one sun illumination (100 mW/cm^2) were investigated by a solar cell I–V measurement system (K3000 LAB, McScience, Korea). Photocurrent density (J_{sc}), open-circuit voltage (V_{oc}), fill factor (FF) and power-conversion-efficiency (η) were simultaneously measured. The incident monochromatic photon-to-current conversion efficiency (IPCE) was recorded as a function of excitation wavelength (λ) by a spectral IPCE measurement system (K3100, McScience, Korea).

3. Results and discussion

3.1. Characterization

Dyes **6** and **7** were conveniently prepared in a two-step protocol from commercially available precursors **1** to **3** (Scheme 1). Sonogashira coupling reactions of compound **1** or **2** with **3** provided compounds **4** and **5**, which upon Knoevenagel condensation with cyanoacetic acid provided dyes **6** and **7**. The UV–vis spectra of compounds **6** and **7** are provided in Fig. 1. The maximum wavelength absorption corresponds to an intramolecular charge-transfer (ICT) between the donor and acceptor groups, whilst the absorption band around 300 nm is likely due to the π–π*

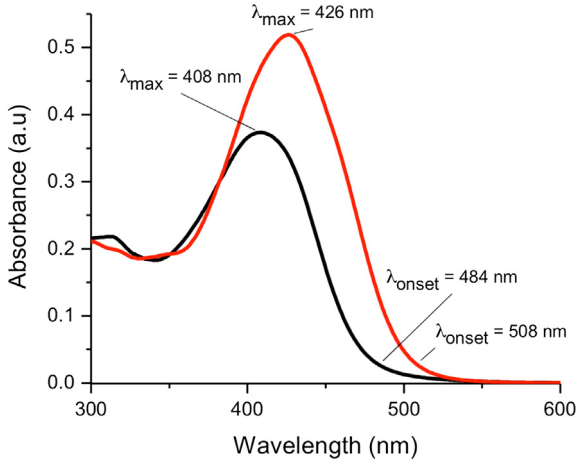

Fig. 1. UV–vis spectra for dyes **6** (black line) and **7** (red line) recorded in DMF (1×10^{-5} M). (For interpretation of the references to color in this figure legend, the reader is referred to the web version of this article.)

transition. It is clear that the addition of the second thiophene moiety in compound **7** induces a bathochromic shift in the longest wavelength absorption of around 18 nm compared to compound **6**, presumably a consequence of extending the conjugation. In addition, the molar extinction coefficient of this absorption is significantly higher for compound **7** (52,000 M^{-1} cm^{-1}) than compound **6** (37,000 M^{-1} cm^{-1}). The optically determined band gaps were 2.56 eV and 2.44 eV for compounds **6** and **7**, respectively, indicating that the addition of the second thiophene unit in the latter is responsible for this decrease. Cyclic voltammetry was used to estimate the HOMO and LUMO energies of the dyes from the oxidation and reduction waves, respectively (Fig. 2). Upon oxidation, both molecules show a reversible oxidation wave (+0.41 V for **6** and +0.36 V for **7**), assigned to the oxidation of the phenylamine unit. Upon reduction, both compounds display an irreversible wave (−2.09 V for **6** and −1.99 V for **7**). The addition of the second thiophene unit in compound **7** lowers the half-wave potential of the oxidation and reduction waves, resulting in a lower band gap for compound **7** (2.36 eV) compared to **6** (2.51 eV). The electrochemically determined band gaps of **6** and **7** are in reasonable accordance with those determined optically. Optical and electrochemical data are summarized in Table 1.

3.2. Computation

To gain insight on the electronic structure and optical properties of our metal-free dyes, DFT and TDDFT calculations were conducted. Ground state optimized geometries gave rise to planar structures for both dyes (Fig. 3). This planarity is likely to contribute to the charge-transfer or separation between the D and A moieties in the molecule as the acetylene and thiophene linker groups help maintain a planar structure whilst increasing the distance between donor and acceptor groups. Moreover, the acetylene linker between phenylamine and thiophene units eliminates the steric hindrance between the hydrogen atoms of these rings. The specific role of acetylene as a π-linker in dyes **6** and **7** was investigated with DFT calculations. Firstly, the acetylene was removed from compounds **6** and **7** and the structures were optimized using the same basis set used above. The resulting energy minimum structures show that the dihedral angle between phenylamine ring and thiophene moieties is 17.2° for **6** and 23.2° for **7** (Fig. 4). The second thiophene group adopts a *trans*-like geometry with respect to the thiophene group nearest to the phenylamine unit. We performed potential energy surface scan upon adjustment of the dihedral angle between two thiophene groups to estimate the relative stability of *trans*- form compared to *cis*-

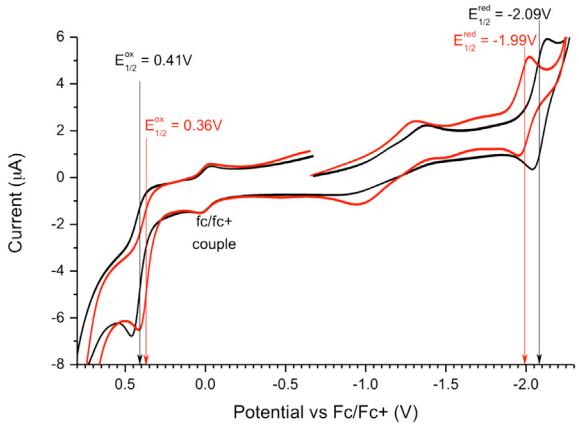

Fig. 2. Cyclic voltammetry of dyes **6** (black line) and **7** (red line) recorded in DMF (5×10^{-4} M). Scan rate = 100 mV/s. (For interpretation of the references to color in this figure legend, the reader is referred to the web version of this article.)

Table 1
Redox and UV–vis properties of dyes **6** and **7**.

	$E_{1/2}$(ox) (V)	$E_{1/2}$(red) (V)	E_{HOMO} (eV)	E_{LUMO} (eV)	E_g (e-chem) (eV)	λ_{max} (nm)	λ_{onset} (nm)	E_g (optical) (eV)
Dye 6	0.41	−2.09	−5.22	−2.71	2.51	408	484	2.56
Dye 7	0.36	−1.99	−5.17	−2.81	2.36	426	508	2.44

structure and as shown in Fig. 5, the energy difference between *these* conformers corresponds to 1.08 kcal/mol, which indicates that around 10% of the *cis* form exists at equilibrium.

The electronic density distributions of the HOMO and LUMO of dyes **6** and **7** are illustrated in Fig. 3. The electron density of the HOMO for the two dyes is localized mainly on the phenylamine moiety (D) and is extended along the alkyne/thiophene bridge to the cyanoacrylic acid (A) moiety. Under light illumination, the intramolecular charge transfer likely occurs from electron donor to electron acceptor. This implies that the HOMO-LUMO excitation would cause a net electron-transfer from the donor to the acceptor group which anchors to the TiO_2 surface [20]. Accordingly, we think that the position of the LUMO close to the anchoring group would enhance the orbital overlap with the Ti 3d orbitals and thus excited electrons can be easily injected into TiO_2 via the cyanoacrylic acid unit. Importantly, the introduction of the second thiophene unit in dye **7** resulted in a more efficient electron transfer from the HOMO of the phenylamine unit to the LUMO of the acrylic acid unit. The molecular orbital (MO) energy levels of the two organic dyes are shown in Fig. 6.

As the number of thiophene π-bridges is increased, the HOMO-LUMO energy gap is decreased, due to an increase in the π-conjugation length, which is in accordance with our spectroscopic data described above. In addition to moving the absorption maximum to longer wavelength, the insertion of the second thiophene introduces larger separation between donor and acceptor unit, which may cause the increase of transition dipole strength, the square of which is proportional to the absorption coefficient. From the TDDFT calculations, we can obtain the transition dipole strength for the HOMO-LUMO transition (Table 2). The absorption spectrum in Fig. 1 shows that the ratio of maximum absorbance is 0.72, which is quite close to the calculated value from the TDDFT. The absorption strength is proportional to the square of the transition dipole which is 0.75. In the above section, charge transfer character is qualitatively described with the electron density map of HOMO and LUMO state. Here, we quantitatively calculate the charge transfer magnitude with the help of TDDFT calculation. The extent of intramolecular charge transfer can be estimated from the difference of dipole moment between ground and excited state [21]. The dipole moment in ground state is obtained by DFT calculation, whereas the excited state by TDDFT calculations. The calculated values for dipole and transition dipole moments are listed in Table 2. The comparison between the dipole moment difference of dye **6** and **7** directly indicates that the insertion of thiophene units enhances the intermolecular charge transfer upon the absorption of light (Fig. 3).

We have also investigated the dye protonation/deprotonation in acetonitrile (the solvent used for deposition of dyes) solution. Recent DFT calculations and FT-IR experiments provides evidence for the coordination of the carboxylate (COO^-) form of the cyanoacrylic acid fragment to titania [22]. Deprotonation of the cyanoacrylic moiety resulted in an increase in the HOMO-LUMO energy gap, suggesting that deprotonation leads to the destabilization of the LUMO and thus the reduction of the electron-acceptor ability of the cyanoacrylic group (Fig. 6). Interestingly, the data obtained for the deprotonated dyes was more in accordance with the HOMO and LUMO energies determined experimentally.

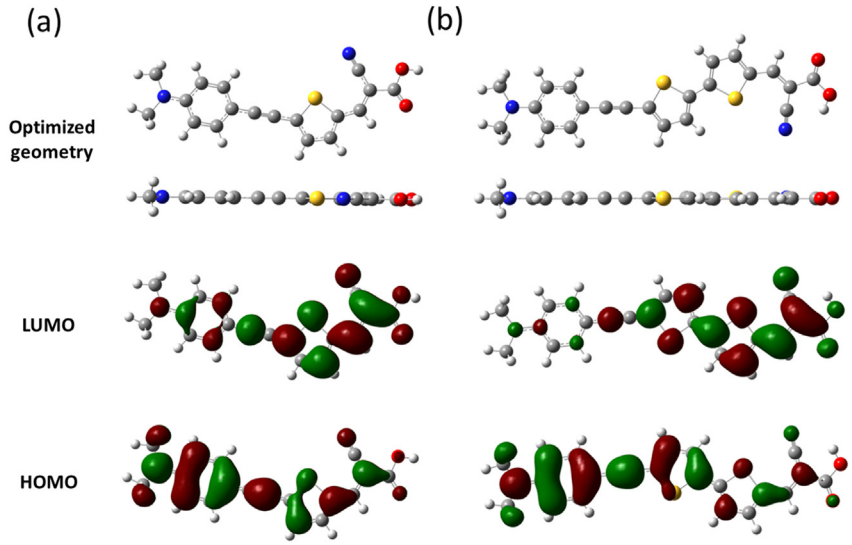

Fig. 3. Optimized structure and frontier molecular orbitals (HOMO and LUMO) of protonated organic dyes: (a) dye **6** and (b) dye **7.**

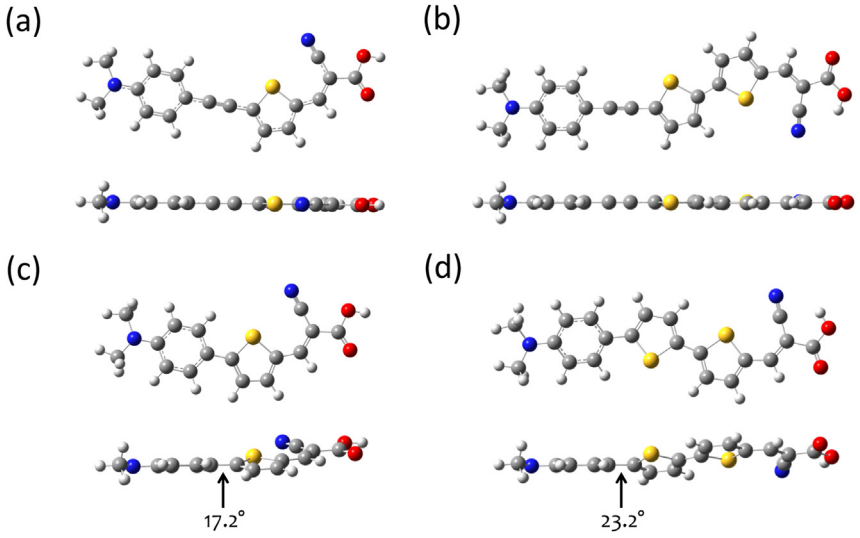

Fig. 4. Geometry of (a) dye **6**, (b) dye **7**, (c) dye **6** (without acetylene spacer) and (d) dye **7** (without acetylene spacer) optimized with Gaussian 09 at the DFT-B3LYP 6-31 + G(d) level of theory.

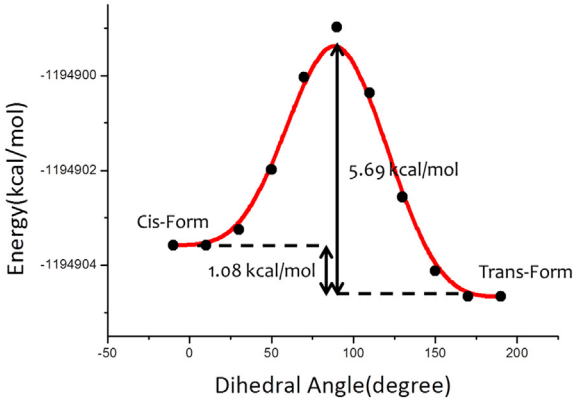

Fig. 5. Energy difference between *trans*- and *cis*-conformers of compound **7** (without acetylene).

3.3. Photovoltaic measurements

Fig. 7 shows *J*–*V* characteristics of DSSCs fabricated from dyes **6** and **7** compared to DSSCs produced from dye **N719** fabricated and measured using the same conditions. The photovoltaic parameters are summarized in Table 3. The addition of the second thiophene bridging unit in dye **7** resulted in better photovoltaic performance: J_{sc} from 7.5 mA/cm^2 to 10.50 mA/cm^2, V_{oc} from 0.61 V to 0.63 V and power η from 3.23% to 4.49%. The increase in η of about 39% can be ascribed to the improvement of the electron-donating ability of this dye compared to **6**. Fig. 8 shows IPCE spectra for DSSCs fabricated from dyes **6**, **7** and **N719**. The IPCE of dye **7** displays a broader band between 300 and 800 nm than that of dye **6**. It is worth noting that dye **7** shows higher maximum IPCE values between 300 and 450 nm than **6** and **N719**. The aforementioned results demonstrate that the addition of the second π-bridge thiophene between the D and A groups broaden the visible absorption spectrum both in solution and upon deposition onto TiO_2 which may be responsible for

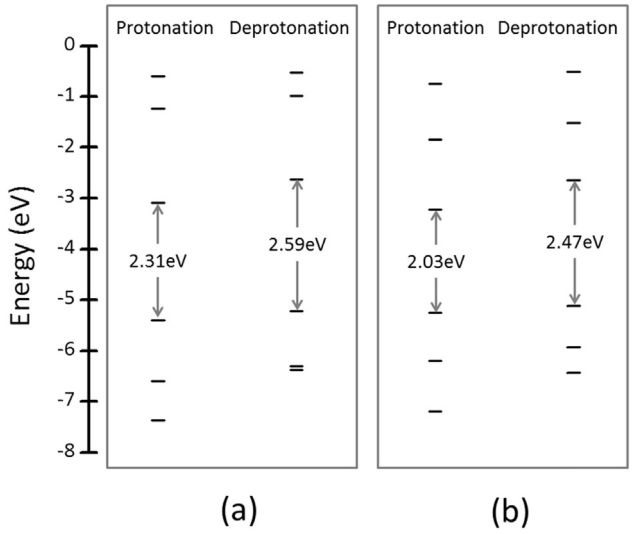

Fig. 6. Comparison between the molecular orbital energy levels of the two organic dyes in acetonitrile solution: (a) dye **6** and (b) dye **7**.

Table 2
Summary of calculated values of dipole and transition dipole moments.

	Ground state (D)	Excited state (D)	Transition dipole moment (a.u.)	Difference (D)
Dye 6	9.63	9.97	18.60	0.34
Dye 7	14.56	12.36	21.38	3.29

$\Delta\mu_{ge} = [(\mu_{gx} - \mu_{ex})^2 + (\mu_{gy} - \mu_{ey})^2 + (\mu_{gz} - \mu_{ez})^2]^{1/2}$

the significant enhancement of DSSC performance (3.23% of dye **6** to 4.49% of dye **7**).

4. Conclusion

In this article, we report the facile synthesis of dyes **6** and **7** in two steps from commercially available materials that have the propensity to form DSSCs with respectable power conversion efficiencies. UV–vis spectroscopy and cyclic voltammetry measurements have shown that the addition of the second thiophene bridge unit in **7** improves both the optical properties of the dye by providing a higher wavelength absorption and consequently a lower band gap than compound **6**. DFT and TDDFT calculations have been performed on the dyes to gain better insight into their structural, electronic and optical properties. The calculations show that the cyanoacrylic acid moiety is coplanar with respect to the acetylene/thiophene bridge, reflecting effective conjugation between these units. Although the efficiencies of dye **6** and **7** were lower than that of the DSSCs fabricated from **N719** (7.65%), we think that through optimization of the device structure (e.g. film thickness, electrolyte, addition of co-additives), improvements in the performance of the DSSCs will result. Nevertheless, the convenient synthesis of these materials and acceptable power conversion efficiencies when incorporated into DSSCs, paves the way for their further development in lower cost photovoltaic applications. Our work towards these goals will be published in due course.

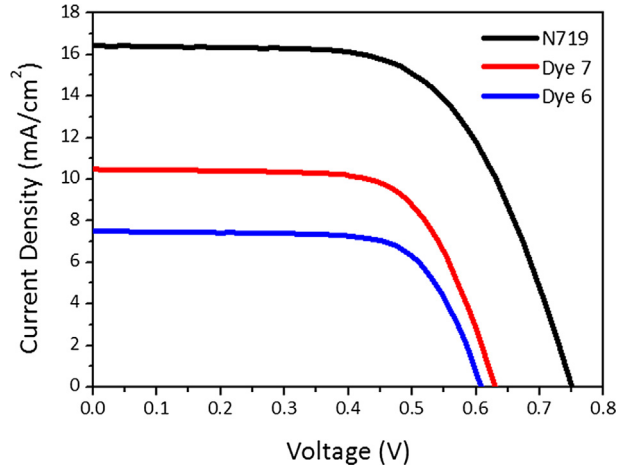

Fig. 7. J-V characteristics of the DSSCs based on dye **6**, dye **7** and **N719**.

Table 3
Photovoltaic performance of DSSCs based on dye **6**, dye **7** and **N719**.

	V_{oc} (V)	J_{sc} (mA/cm^2)	FF (%)	η (%)
Dye 6	0.61	7.5	70.7	3.23
Dye 7	0.63	10.5	67.7	4.49
N719	0.75	16.4	61.9	7.65

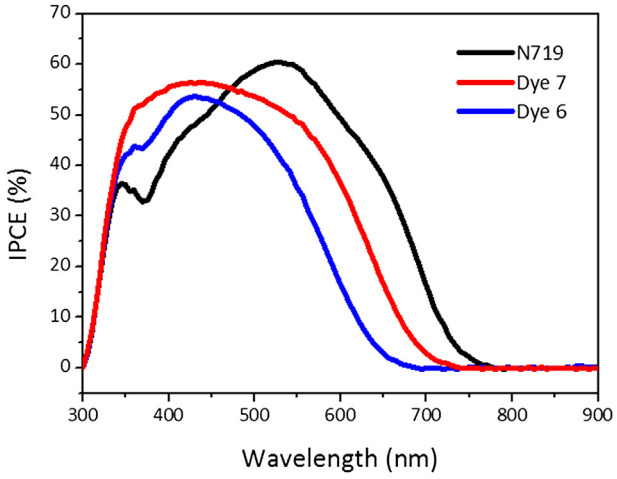

Fig. 8. IPCE spectra of the DSSCs based on dye **6**, dye **7** and **N719**.

Acknowledgements

MA-E thanks the Ministry of Higher Education (Saudi Arabia) for a scholarship. BF and GC thank the EPSRC. JH acknowledges Basic Science Research Program (2013-026989) and Mid-career Research Program (2012-047815) through the National Research Foundation (NRF) funded by the Ministry of Science, ICT & Future Planning (MSIP) of Korea. KW acknowledges the Chung-Ang University Excellent Student Scholarship. KK thanks for the support from Basic Science Research Program through the NRF funded by the MSIP of Korea (2009-0093817).

References

[1] Hagfeldt A, Boschloo G, Sun L, Kloo L, Pettersson H. Dye-sensitized solar cells. Chem Rev 2010;110:6595–663.
[2] Robertson N. Optimizing dyes for dye-sensitized solar cells. Angew Chem Int Ed 2006;45:2338–45.
[3] Mishra A, Fischer MKR, Bäuerle P. Metal-free organic dyes for dye-sensitized solar cells: from structure: property relationships to design rules. Angew Chem Int Ed 2009;48:2474–99.
[4] Ooyama Y, Harima Y. Photophysical and electrochemical properties, and molecular structures of organic dyes for dye-sensitized solar cells. ChemPhysChem 2012;13:4032–80.
[5] Kanaparthi RK, Kandhadi J, Giribabu L. Metal-free organic dyes for dye-sensitized solar cells. Tetrahedron 2012;68:8383–93.

[6] Wu Y, Zhu W. Organic sensitizers from D–π–A to D–A–Pπ–A: effect of the internal electron-withdrawing units on molecular absorption, energy levels and photovoltaic performances. Chem Soc Rev 2013;42:2039–58.
[7] Kim B-G, Chung K, Kim J. Molecular design principle of all-organic dyes for dye-sensitized solar cells. Chem Eur J 2013;19:5220–30.
[8] Yella A, Lee H-W, Tsao HN, Yi C, Chandiran AK, Nazeeruddin MK, et al. Porphyrin-sensitized solar cells with cobalt (II/III)–based redox electrolyte exceed 12 percent efficiency. Science 2011;334:629–34.
[9] Olivier C, Sauvage F, Ducasse L, Castet F, Grätzel M, Toupance T. Fine-tuning of triarylamine-based photosensitizers for dye-sensitized solar cells. ChemSusChem 2011;4:731–6.
[10] Kim S, Lee JK, Kang SO, Ko J, Yum J-H, Fantacci S, et al. Molecular engineering of organic sensitizers for solar cell applications. J Am Chem Soc 2006;128:16701–7.
[11] Jung HS, Lee J-K. Dye sensitized solar cells for economically viable photovoltaic systems. J Phys Chem Lett 2013;4:1682–93.
[12] Song J-L, Amaladass P, Wen S-H, Pasunooti KK, Li A, Yu Y-L, et al. Aryl/heteroarylethyne bridged dyes: the effect of planar π-bridge on the performance of dye-sensitized solar cells. New J Chem 2011;35:127–36.
[13] Teng C, Yang X, Yang C, Tian H, Li S, Wang X, et al. Influence of triple bonds as π-spacer units in metal-free organic dyes for dye-sensitized solar cells. J Phys Chem C 2010;114:11305–13.
[14] Srinivas K, Kumar CR, Reddy MA, Bhanuprakash K, Rao VJ, Giribabu L. D–π–A organic dyes with carbazole as donor for dye-sensitized solar cells. Synth Met 2011;161:96–105.
[15] Kivala M, Diederich F. Acetylene-derived strong organic acceptors for planar and nonplanar push-pull chromophores. Acc Chem Res 2009;42:235–48.
[16] Pommerehne J, Vestweber H, Guss W, Mahrt RF, Bässler H, Porsch M, et al. Efficient two layer LEDs on a polymer blend basis. Adv Mater 1995;7:551–4.
[17] Frisch MJ, Trucks GW, Schlegel HB, Scuseria GE, Robb MA, Cheeseman JR, et al. Gaussian 09. Wallingford CT: Gaussian, Inc.; 2009.
[18] Koo H-J, Velev OD. Regenerable photovoltaic devices with a hydrogel-embedded microvascular network. Sci Rep 2013;3:2357.
[19] Ito S, Chen P, Somte P, Nazeeruddin MK, Liska P, Pechy P, et al. Fabrication of screen-printing pastes from TiO_2 powders for dye-sensitized solar cells. Prog Photovolt Res Appl 2007;15:603–12.
[20] Hardin BE, Snaith HJ, McGehee MD. The renaissance of dye-sensitized solar cells. Nat Photonics 2012;6:162–9.
[21] Rolczynski BS, Szarko JM, Son HJ, Liang Y, Yu L, Chen LX. Ultrafast intramolecular exciton splitting dynamics in isolated low-band-gap polymers and their implications in photovoltaic materials design. J Am Chem Soc 2012;134:4142–52.
[22] Pasture M, Angelis FD. Intermolecular interactions in dye-sensitized solar cells: a computational modeling perspective. J Phys Chem Lett 2013;4:956–74.